Directing Droplets Using Microstructured Surfaces†

Ashutosh Shastry,* Marianne J. Case, and Karl F. Böhringer

Department of Electrical Engineering, University of Washington, Seattle, Washington 98195

Received January 17, 2006. In Final Form: March 8, 2006

Systematic variation of microscale structures has been employed to create a rough superhydrophobic surface with a contact angle gradient. Droplets are propelled down these gradients, overcoming contact angle hysteresis using energy supplied by mechanical vibration. The rough hydrophobic surfaces have been designed to maintain air traps beneath the droplet by stabilizing its Fakir state. Dimensions and spacing of the microfabricated pillars in silicon control the solid−liquid contact area and are varied to create a gradient in the apparent contact angle. This work introduces the solid−liquid contact area fraction as a new control variable in any scheme of manipulating droplets, presenting theory, fabricated structures, and experimental results that validate the approach.

1. Introduction

Microscale bioanalysis is pregnant with assay possibilities that are potentially useful in diagnostic applications and as research tools for biologists. Continuous flow systems have been the default approach toward such lab-on-chip bioassay systems. Droplet-based lab-on-chip applications have become increasingly popular, however, because they enable spatially and temporally resolved chemistries.[2] Employing surface-energy gradients to cause the movement of droplets has been the common theme of several apparently disparate actuation approaches.[3] These surface-energy gradients can be categorized into static or hard-coded and dynamic or "programmable". Electrowetting is an example of a programmable surface-energy gradient.[4,5] There are other instances where the gradient tracks are hard-coded but the actuation is programmable,[6,7] employing the Marangoni effect for droplet actuation. The droplet is confined to a hard-coded hydrophilic track and propelled along by a dynamic temperature gradient.

Chaudhary and Whitesides[8] created a passive contact angle gradient by reacting silicon with the diffusing front of alkyltrichlorosilane, generating a gradually varying chemical composition along the length of the surface. The highlight of the work was the very low hysteresis surface that ensured that the force of the gradient alone was sufficient to move the droplet against gravity. Using similar chemical gradients, Daniel et al. actuated the droplets harnessing alternative sources of energy to overcome the impeding force of contact angle hysteresis. In one case, the energy released by the condensation of steam propelled the drops along radial energy gradients,[9] whereas acoustic vibration was employed in other cases.[10,11] Bain et al.[12] introduced dynamic gradients formed by the continuous chemical reaction of hydrophobic alkyl silanes inside the droplet with the solid surface. Thiele et al.[13] further explored such dynamic gradients through modeling and experiments.

In recent years, there have been remarkable advances in our understanding of the wetting of textured surfaces.[14,15] Mahadevan introduced the term "Fakir",[16] and later Quéré used it to describe droplets resting on rough surfaces with air pockets trapped beneath them.[17] These trapped air pockets ensure a low solid−liquid contact area fraction and significantly reduced drag,[19,20] allowing droplets to be moved on the surface with low amounts of energy.[21] Fakir droplets are very stable on superhydrophobic nanorough surfaces—they are able to resist collapsing under large pressures.[22] Their stability and low resistance to flow make Fakir droplets attractive candidates for any low-energy droplet manipulation scheme. Petrie et al.[23] recently reported the first efforts to manipulate these Fakir droplets, employing Chaudhary's static chemical gradient approach on a nanorough surface that stabilizes Fakir droplets. Lee et al.[24] have recently reported a device that switches the roughness of a membrane to move a droplet.

We demonstrate, for the first time, droplets moving down surface-energy gradients created by systematically varying the solid−liquid area fraction of Fakir droplets.[1] We start with a short review of the theory of wetting of rough surfaces and droplet movement due to contact angle gradients. We combine the two theories to propose a model that predicts conditions for the incipient motion of droplets on roughness-controlled gradient tracks. Next, we outline our design approach, fabrication process,

† Preliminary results from section 5.1 were presented at the IEEE International Conference on MEMS in Jan 2005.[1]

* Corresponding author. E-mail: ashutosh@washington.edu. Phone: (206) 543 5218.

(1) Shastry, A.; Case, M. J.; Böhringer, K. F. Engineering Surface Roughness to Manipulate Droplets in Microfluidic Systems. 18th IEEE International Conference on Micro Electro Mechanical Systems, Miami, FL, 2005.
(2) Stone, H. A.; Stroock, A. D.; Ajdari, A. *Annu. Rev. Fluid Mech.* **2004**, *36*, 381−411.
(3) Darhuber, A. A.; Troian, S. M. *Annu. Rev. Fluid Mech.* **2005**, *37*, 425−455.
(4) Mugele, F.; Baret, J. C. *J. Phys.: Condens. Matter* **2005**, *17*, R705−R774.
(5) Pollack, M.; Fair, R.; Shenderov, A. *Lab Chip* **2002**, *2*, 96−101.
(6) Kataoka, D. E.; Troian, S. M. *Nature* **1999**, *402*, 794−797.
(7) Brochard, F. *Langmuir* **1989**, *5*, 432−438.
(8) Chaudhary, M. K.; Whitesides, G. M. *Science* **1992**, *256*, 1539−1541.
(9) Daniel, S.; Chaudhury, M. K. Chen, J. C. *Science* **2001**, *291*, 633−636.
(10) Daniel, S.; Chaudhury, M. K. *Langmuir* **2002**, *18*, 3404−3407.
(11) Daniel, S.; Sircar, S.; Gliem, J.; Chaudhury, M. K. *Langmuir* **2004**, *20*, 4085−4092.
(12) Bain, C. D.; Burnett-Hall, G. D.; Montgomerie, R. R. *Nature* **1994**, *372*, 415−416.
(13) Thiele, U.; John, K.; Bär, M. *Phys. Rev. Lett.* **2004**, *93*, 027802-1−027802-4.
(14) Bico, J.; Marzolin, C.; Quéré, D. *Europhys. Lett.* **1999**, *47*, 220−226.
(15) Bico, J.; Thiele, U.; Quéré, D. *Colloids Surf., A* **2002**, *206*, 41−46.
(16) Mahadevan, L. *Nature* **2001**, *411*, 895−896.
(17) Quéré, D. *Nat. Mater.* **2002**, *14*, 1109−1112.
(18) Lafuma, A.; Quéré, D. *Nat. Mater.* **2003**, *2*, 457−460.
(19) Cottin-Bizonne, C.; Barrat, J. L.; Bocquet, L.; Charlaix, E. *Nat. Mater.* **2003**, *2*, 237−240.
(20) Choi, C. H.; Kim, C. J. Measurement of Slip on Nanotur Surfaces. Proceedings of ASME 2005: Integrated Nanosystems Design, Synthesis & Applications, Berkeley, CA, 2005.
(21) Quéré, D.; Lafuma, A.; Bico, J. *Nanotechnology* **2003**, *1*, 14−15.
(22) Journet, C.; Moulinet, S.; Ybert, C.; Purcell, S. T.; Bocquet, L. *Europhys. Lett.* **2005**, *71*, 104−109.
(23) Petrie, R. J.; Bailey, T.; Gorman, C. B.; Genzer, J. *Langmuir* **2004**, *20*, 9893−9896.
(24) Lee, J.; He, B.; Patankar, N. A. *J. Micromech. Microeng.* **2005**, *15*, 591−600.

10.1021/la0601657 CCC: $33.50
Published on Web 06/09/2006

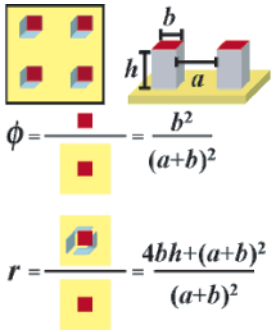

Figure 1. Texture parameters ϕ and r expressed in terms of design parameters a (gap length), b (pillar size), and h (pillar height), where ϕ is the fraction of the pillar top area over the total horizontal surface area and r is the fraction of the total surface area over the total horizontal surface area. The value ϕ determines the apparent contact angle θ_F as given by eq 3. The value r correlates with the relative stability of a droplet in the Fakir state as opposed to the Wenzel state.

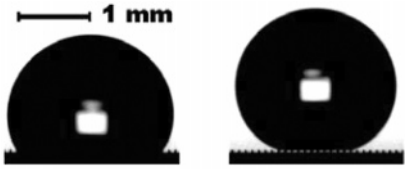

Figure 2. Droplets of volume 5 μL on a Teflon-coated silicon surface with $\phi = 0.05$ and $r = 1.4$ in (a) the Wenzel state with a footprint diameter of 1.96 mm, $\theta_W = 118°$ (expected, 112.8°) and (b) the Fakir state with a footprint diameter of 1 mm, $\theta_F = 156.6°$ (expected, 164.5°). Air pockets are visible between pillars under the Fakir-state droplet. In our experiments as shown in these figures, pinning of the droplet edge caused significant deviations from the predicted equilibrium value.

and experimental setup. Finally, we present results and observed trends and compare them with the theoretical predictions based on our model. We conclude by pointing out the implications of this work and resulting directions that emerge as worthwhile pursuits.

2. Theory and Model

We begin by reviewing the theory of wetting of rough surfaces. Then we develop a model of the forces acting on the droplet resting on a roughness-controlled contact angle gradient. Next, we use this model to estimate the minimum slope required for the droplet to move without the need for external forces.

2.1. Review of the Wetting of Rough Surfaces. Consider a rough surface realized by creating pillars of controlled geometry on a smooth surface. Here the roughness is characterized by r, the ratio of rough to planar surface area, as explained in Figure 1. The basic effect of surface roughness on wetting is modeled by Wenzel's relation (eq 1), which relates the apparent contact angle θ_W of a droplet on a rough surface with $r \geq 1$ to Young's intrinsic contact angle θ_i.[25]

$$\cos \theta_W = r \cos \theta_i \tag{1}$$

In the Wenzel state, the droplet is conformal with the topography, as seen in Figure 2a. The droplet can also sit on the pillar tops with air pockets trapped beneath it, as shown in Figure 2b. This configuration is referred to as the "Fakir" state. In the

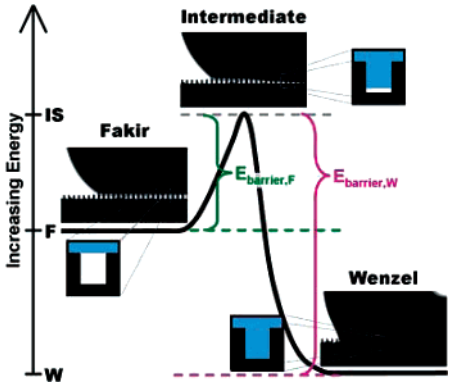

Figure 3. Schematic showing energy levels of the Fakir and Wenzel states. The choice of texture parameters makes the Fakir state metastable in this example. The energy of the intermediate state is calculated by assuming nearly complete penetration of the droplet; only a thin film of air separates the liquid−air and solid−air interfaces at the bottoms of the valleys. A Fakir droplet needs to overcome the energy barrier $E_{barrier,F} = E_{IS} - E_F$ to move to the Wenzel state.

Fakir state, the base of the droplet essentially contacts a composite surface of pillar tops and air. The apparent contact angle θ_{CB} on a composite surface is determined using the Cassie−Baxter relation given in eq 2

$$\cos \theta_{CB} = \sum \phi_j \cos \theta_j \tag{2}$$

where ϕ_j is the surface area fraction and θ_j is the intrinsic contact angle of material j with water.

For a sessile Fakir droplet, a surface area fraction ϕ (Figure 1) of its base rests on pillar tops that have an intrinsic contact angle of θ_i; the remaining surface area fraction of $(1 - \phi)$ is freely suspended and is in contact with air with a contact angle of 180°. Substituting these values, the apparent contact angle in the Fakir state, a special case of Cassie−Baxter contact, is readily computed[14,15] to yield eq 3.

$$\cos \theta_F = \phi(\cos \theta_i + 1) - 1 \tag{3}$$

Angles θ_F from eq 3 and θ_W from eq 1 are *equilibrium* values of the apparent contact angle in the two states. Equilibrium angles of the droplet are expected when there is *no* impending movement. Even under these conditions, there are significant fluctuations of the measured contact angle, also called contact angle hysteresis,[26] when the two energy levels are close. Contact-angle hysteresis is defined as the difference between the cosines of maximum advancing and minimum receding angles that a droplet makes with a surface. Hysteresis results from the pinning of the three-phase contact line to the solid surface and is attributed to physical and chemical inhomogeneities.[25] We also notice by comparing θ_F from eq 3 and θ_W from eq 1 that the Fakir state has a lower energy relative to the Wenzel state (i.e., $\cos \theta_W < \cos \theta_F$) if the following inequality proposed by Bico et al.[15] (eq 4) holds true.

$$\cos \theta_i < \frac{\phi - 1}{r - \phi} \tag{4}$$

A droplet at a given location on a surface does not spontaneously transit from one state to the other because of the presence of an energy barrier. This energy barrier is analogous to the activation energy of a chemical reaction that prevents spontaneous conversion to products (Figure 3). This energy barrier is easily

(25) de Gennes, P. G.; Brochard-Wyart, F.; Quéré, D. *Capillarity and Wetting Phenomena: Drops, Bubbles, Pearls, Waves*; Springer: New York, 2004.

(26) Lafuma, A.; Quéré, D. *Nat. Mater.* **2003**, *2*, 457−460.

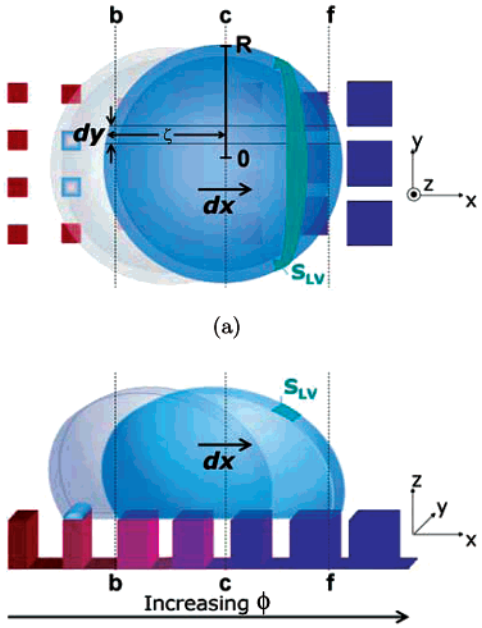

Figure 4. Droplet slice of width *dy* shown moving a length *dx* down a contact angle gradient: (a) top view and (b) side view. The previous location of the droplet is shown in light gray. A film is left behind on previous pillars as shown, and the front area of the droplet increases by S_{LV}, which is represented by a teal patch.

estimated.[27] In situations where eq 4 does not hold, the energy barrier gives a useful bound on the energy that needs to be coupled to a Fakir droplet before risking its transition to the Wenzel state.

2.2. Model for the "Slope" Required for Incipient Movement. Let us examine a sessile droplet at rest on a horizontal hydrophobic surface. The total energy U of a droplet is the sum of two components: U_γ due to its interfaces and U_g due to its position in a force field of body forces acting on it. We consider a small water droplet of radius $R < \kappa^{-1}$ where ρ is the density, g is the acceleration due to gravity, γ_{LV} is the surface tension of the liquid, and κ^{-1} is the capillary length $\sqrt{\gamma_{LV}/\rho g}$. For water, κ^{-1} is 2.7 mm, corresponding to approximately 80 μL of water in a spherical drop. For droplets smaller than 80 μL, gravity has a negligible effect on shape, and the droplet can be approximated as a spherical cap. In the absence of any body forces, $U_g \equiv 0$ and the following equation (eq 5) is true.

$$U = U_\gamma = A_{SL}\gamma_{SL} + A_{SV}\gamma_{SV} + A_{LV}\gamma_{LV} \tag{5}$$

When the droplet rests on a surface energy gradient, it experiences a driving force. Spontaneous movement down the gradient is impeded, however, by the opposing force due to contact angle hysteresis. When an external force is applied to mitigate hysteresis, the droplet moves down the surface energy gradient, overcoming pinning. When the droplet is in motion, the viscous drag adds to the hysteresis force to oppose the driving force. But under the condition of incipient motion, which occurs just before the droplet moves, viscous drag is nonexistent, and the driving force equals the hysteresis force.

Let us consider the droplet shown in Figure 4. The height of the droplet slice is a function of the x coordinate only. A slice of liquid of width dy experiences a driving force parallel to x, following Brochard.[7] The slice occupies an interval $x_b < x < x_f$. The following equation (eq 6) represents the force balance under the condition of incipient movement of the slice:

$$dU_{net,slice} = \gamma_{LV}(\cos\theta_{b,r} - \cos\theta_{f,a})\,dxdy = 0 \tag{6}$$

Since the contact angles of the two edges are equal, there is no pressure gradient and hence no flow at the threshold of movement. The threshold condition represents an equilibrium between the driving force and hysteresis force such that the net force is zero:

$$\begin{aligned}\frac{dU_{net,slice}}{dx} &= \gamma_{LV}\Big[\underbrace{(\cos\theta_b - \cos\theta_f)dy}_{driving\ force} \\ &\quad + \underbrace{\overbrace{(\cos\theta_{b,r} - \cos\theta_b)\,dy}^{hysteresis,\ back\ edge} + \overbrace{(\cos\theta_f - \cos\theta_{f,a})\,dy}^{hysteresis,\ front\ edge}}_{hysteresis\ force}\Big] \\ &= 0\end{aligned} \tag{7}$$

To model the incipient motion of the droplets, we need to express each term in eq 7 as a function of surface parameters and integrate it over the footprint of the droplet. In the absence of rigorous theoretical models for θ_r and θ_a on rough hydrophobic surfaces, we employ the heuristic relations available from the literature to predict the bounds of advancing and receding contact angles after having experimentally validated them.[30]

To obtain θ_r, we follow the approach of Fort and Roura[28,29] who postulate that a thin film of liquid is left behind as shown in Figure 4. This assumption, originally proposed for hydrophilic surfaces,[28] expectedly overestimates hysteresis, providing an upper bound for hydrophobic surfaces, except for the low ϕ regime.

To obtain θ_a, we consider a droplet moving forward while its three phase contact line remains pinned, resulting in an advancing angle instead of the equilibrium angle at the front edge. The deviation from the equilibrium value is captured through a factor S_{LV} which equals $\cos\theta - \cos\theta_a$ and accounts for the increased liquid−vapor interface shown in Figure 4 at the front edge. It is also the measure of energy required for depinning. Once the maximum advancing angle is reached, the edge gets depinned and advances.

To estimate the driving force, we displace the whole slice by dx and write an expression for the variation of interfacial energy dU. The expression for the differential energy dU of the slice follows in eq 8:

$$\begin{aligned}dU &= \underbrace{\phi_b(\gamma_{SL} - \gamma_{SV} + \gamma_{LV})}_{film}\,dxdy \\ &\quad - \underbrace{\Big((1-\phi_b)\gamma_{LV} + \phi_b(\gamma_{SL} - \gamma_{SV})\Big)}_{back\ edge}\,dxdy \\ &\quad + \underbrace{\Big((1-\phi_f)\gamma_{LV} + \phi_f(\gamma_{SL} - \gamma_{SV})\Big)}_{front\ edge}\,dxdy + \underbrace{(S_{LV}\gamma_{LV})}_{pinning}\,dxdy\end{aligned} \tag{8}$$

ϕ_f and ϕ_b are values of ϕ at the front and back edges of the droplet, respectively, and the interfacial energy symbols γ_{ij} maintain their previously defined meanings.

(27) Patankar, N. A. *Langmuir* **2004**, *20*, 7097−7102.

(28) Roura, P.; Fort, J. *Phys. Rev. E* **2001**, *64*, 011601.

(29) Roura, P.; Fort, J. *Langmuir* **2002**, *18*, 566−569.

(30) Shastry, A.; Goyal, S.; Epilepsia, A.; Case, M. J.; Abbasi, S.; Ratner, B. D.; Böhringer, K. F. *Engineering Surface Micro-structure to Control Fouling and Hysteresis in Droplet based Microfluidic Bioanalytical Systems*. In the Technical Digest of the 12th Solid State Sensor, Actuator and Microsystems Workshop, Hilton Head, June 4−8, 2006.

Next we use Young's equation ($\cos\theta_i = (\gamma_{SV} - \gamma_{SL})/\gamma_{LV}$) and rearrange eq 8 to obtain the following expression (eq 9) for the net force on the slice, $F_{net,slice}$.

$$F_{net,slice} = -\frac{dU}{dx} = -\gamma_{LV}\left[\underbrace{(2\phi_b - 1)}_{\cos\theta_{b,r}} - \underbrace{(-1 + \phi_f(\cos\theta_i + 1)}_{\cos\theta_f} - S_{LV})\right]dy \quad (9)$$

The first term ($2\phi_b - 1$) equals $\cos\theta_{b,r}$, where $\cos\theta_{b,r}$ is the receding angle of the back edge of the droplet as obtained by Patankar.[31] As mentioned earlier, recent experimental study by Shastry et al.[30] shows that this model provides an upper bound for $\phi > 0.1$.

In the absence of models to predict S_{LV}, we substitute it with $\cos\theta_F - \cos\theta_{F,a}$ and employ the heuristic relation proposed by He et al.[32] given in eq 10 for the advancing contact angle $\theta_{F,a}$ of a Fakir droplet

$$\cos\theta_{F,a} = -1 + \phi_F(\cos\theta_{i,a} + 1) \quad (10)$$

where $\theta_{i,a}$ is the advancing contact angle on a smooth surface. We then write $F_{net,slice}$, in terms of ϕ and the intrinsic contact angle θ_i by starting with eq 7, using the contact angle for the Fakir droplet (eq 3), and substituting for $\cos\theta_{f,a}$ from eq 10 and $\cos\theta_{b,r}$ from eq 9 to obtain eq 11.

$$F_{net,slice} = \gamma_{LV}\left[\underbrace{(\phi_f - \phi_b)(\cos\theta_i + 1)dy}_{driving\ force} \underbrace{-\left((\phi_f - \phi_b)\cos\theta_i - (\phi_f\cos\theta_{i,a} - \phi_b)\right)dy}_{hysteresis\ force}\right] \quad (11)$$

At this stage, we have expressions for the driving force and hysteresis force on the slice as functions of ϕ_f and ϕ_b. We need to express ϕ_f and ϕ_b as functions of the position of the droplet on the gradient. We do so by utilizing the constant slope of the gradient tracks an approach parallel to those of Brochard[7] and Daniel et al.[10] Let ϕ_c be the value of ϕ at x_c, the center of the slice that occupies an interval $x_b < x < x_f$. For the slice, $x_b = x_c - \zeta$ and $x_f = x_c + \zeta$, hence $-(d\phi/dx)2\zeta = (\phi_b - \phi_f)$. The following substitutions can therefore be made.

$$\phi_b = \phi_c(x) - \frac{d\phi}{dx}\zeta \quad (12)$$

$$\phi_f = \phi_c(x) + \frac{d\phi}{dx}\zeta \quad (13)$$

We have thus expressed forces on a slice in terms of its location on the gradient. To estimate forces on the entire droplet, we integrate these forces over the range of y, which is $2R$, the diameter of the footprint of the droplet, noting that the slope $d\phi/dx$ is a constant.

$$F_{net,droplet} = 2\int_0^R \frac{F_{net,slice}}{dy}\,dy \quad (14)$$

(31) Patankar, N. A. *Langmuir* **2003**, *19*, 1249−1253.
(32) He, B.; Lee, J.; Patankar, N. A. *Colloids Surf., A* **2004**, *248*, 101−104.

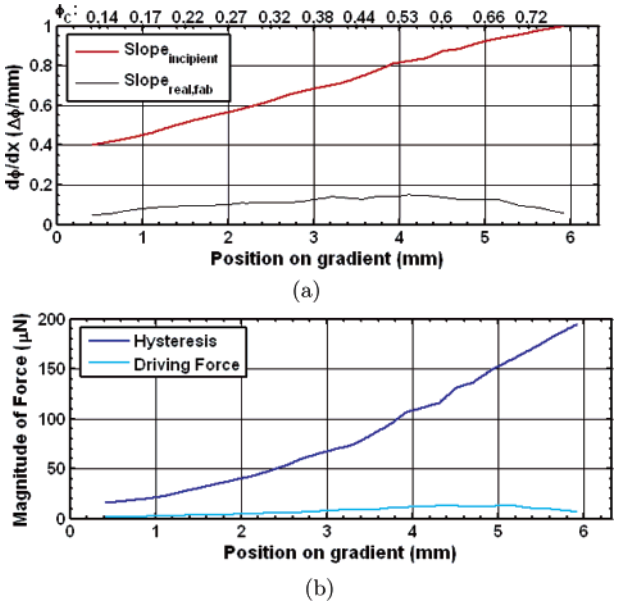

Figure 5. Teflon-coated continuous gradient with $\theta_i = 115°$. The values of intrinsic advancing and receding angles used in the hysteresis model were the measured values $\theta_{i,r} = 113°$ and $\theta_{i,a} = 160°$. (a) The slope required for incipient motion given ϕ_c at location x_c on the gradient and the actual slope of the gradient at each position x_c are plotted for a 5 μL droplet. (b) For the same gradient and droplet volume, the magnitudes of the driving force $F_d(x)$ and hysteresis force $F_{hyst}(x)$ as obtained from eq 16 are shown.

Now substituting for $F_{net,slice}$ from eq 11, we obtain the following (eq 15)

$$F_{net,droplet} = \underbrace{4\gamma_{LV}\frac{d\phi}{dx}(\cos\theta_i + 1)\int_0^R \zeta(y)dy}_{driving\ force} \underbrace{-2\gamma_{LV}C\int_0^R \zeta(y)dy - 2\gamma_{LV}\phi_c(1 - \cos\theta_{i,a})\int_0^R dy}_{hysteresis\ force} \quad (15)$$

where $C = (d\phi/dx)(2\cos\theta_i - 1 - \cos\theta_{i,a})$

The final force expression is thus obtained (eq 16).

$$F_{net,droplet} = \underbrace{\gamma_{LV}\frac{d\phi}{dx}(\cos\theta_i + 1)\pi R^2}_{F_d,\ driving\ force} \underbrace{-\frac{C}{2}\gamma_{LV}\pi R^2 - \gamma_{LV}\phi_c(1 - \cos\theta_{i,a})2R}_{F_{hyst},\ hysteresis\ force} \quad (16)$$

It is important to notice that R depends on both droplet volume V and location x_c depends on the gradient. R is approximated by the following equation (eq 17).

$$R = \sin\theta_c\left(\frac{3V}{\pi(\cos^3\theta_c - 3\cos\theta_c + 2)}\right)^{1/3} \quad (17)$$

A plot of these force contributions as a function of position for a typical gradient is shown in Figure 5b.

3. Design and Fabrication

3.1. Design. We have developed chemically homogeneous but textured surfaces. A regular two-dimensional array of square pillars created a rough surface. The dimensions of the surface, with gap length a and pillar width b, were varied spatially across distances ranging from 4 to 8 mm to produce several texture gradients with uniform linear changes in $\cos\theta_F$ along their length

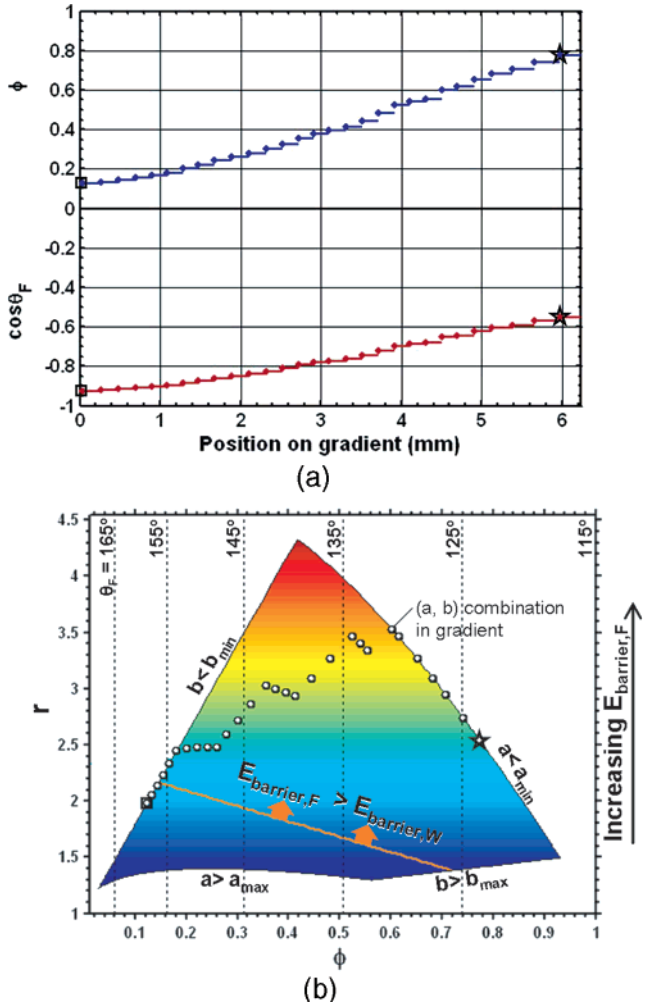

Figure 6. (a) Contact angle gradient having an approximately constant slope ($d \cos \theta_F)/dx$. The minimum and maximum contact angles were determined by the limits of the design space, using $\theta_{i,a} = 115°$ for Teflon. Pillar widths and gaps were specified to create a gradient of specified length between the two end points. (b) Contour plot showing the possible gap length and pillar width combinations within the constraints imposed by design and fabrication. Vertical isolines represent combinations of constant θ_F. Isocolors specify combinations with constant $E_{barrier,F}$. The bold orange line signifies the combinations for which $E_{barrier,W} = E_{barrier,F}$, as given by eq 4. It is desirable to maintain $E_{barrier,F} > E_{barrier,W}$ to ensure that Fakir droplets remain stable.

(Figure 6a). In some cases, a steeper slope was used on the latter section of the gradient to mitigate the increasing hysteresis force associated with larger ϕ values.

Fabrication constraints and design requirements decided the limits of ϕ, ϕ_{min}, and ϕ_{max}. The constraints on the design space are explained in Figure 6b. The desired cos θ_F at each location along the gradient was a function of the intended gradient length and slope. Actual gradient length and slope varied slightly depending on the (a, b) combinations employed. As seen in Figure 6b, each desired contact angle can be realized using several (a, b) combinations. Because the resolution of the photolithography mask was limited to 1 μm, the most precise values of (a, b) are those close to whole micrometer values. The most stable (a, b) combinations allowed by this resolution constraint were selected.

3.2. Fabrication. The pillar dimensions and spacings obtained as vectors $a(x)$ and $b(x)$ defined the gradients. Layouts of these gradients were drafted using L-Edit. Transparency photomasks were printed at CAD/Art Services Inc. (Figure 7a). We used N-type ⟨100⟩ silicon wafers as the substrate. Photolithography was performed using an AZ4620 photoresist. Next, pillars were etched using the standard Bosch process for deep reactive ion etching (DRIE). The etch depth defined pillars of height 40 μm.

The SEM micrograph in Figure 7c shows etched pillars after stripping the resist slice. The rough surfaces were then coated with an adhesion-promoting silane and finally with Teflon AF1600 to obtain the hydrophobic layer.

4. Setup and Experiment

The experimental setup is shown in Figure 8. A gradient die was secured to a stage using double-sided tape. The stage was glued to the diaphragm of a speaker, which was in turn connected to a function generator (Agilent 33120A). A square wave (typically 20 Hz, 50 mV) was applied to the speaker using the function generator, causing the stage to vibrate vertically with a typical amplitude of 180 μm as shown in Figure 8. Water droplets ranging from 2 to 10 μL were deposited at the beginning of the gradient using a hand syringe. The droplet was illuminated with a 300 W halogen lamp (Gemini high-intensity light source) directed through an optical fiber bundle. There was no observable evaporation of the droplet during the time it took the droplet to move down the gradient ($<$1−8 s). A high-speed camera (Lightning RDT, Data and Imaging Systems) recorded the movement at 500 frames/s.

5. Results and Discussion

We first present proof-of-principle results to validate the basic hypothesis. We then present other salient observations. We create plots of theoretical predictions using our model, compare them with experimental results, and explain the trends.

5.1. Gradients Guide Droplets. Vibration provided the force required to overcome pinning and allowed the bases of the droplets to "explore" their vicinity and sense the gradients. Droplets then moved down the gradients. Alternatively, we can summarize the phenomenon as texture-controlled gradients rectifying the random motion of droplets caused by vibration. To ascertain that the gradient and not the stage tilt or vibration bias directed the droplet, we designed a control experiment.

For the control experiment, two similarly sized droplets were placed on oppositely oriented gradients on the same die. When vibrated, these Fakir droplets moved as expected, in opposite directions down their respective gradients (Figure 9). Thus, the proof-of-principle was established: roughness-controlled gradients can direct Fakir droplets.

The frame that showed the first observable displacement of the stage marked the beginning of the experiment and was assigned as $t = 0$. The stage height along with the droplet position and its height were determined in each frame using an image analysis program that we developed in Matlab. For one such run, Figure 10a shows the position of a 5 μL droplet on the gradient every 2 ms. It illustrates different phases of the journey on the continuous gradient: acceleration, uniform velocity, deceleration, and an eventual halt. Figure 10b shows the average over eight such runs of a 5 μL droplet. Two observations were made: that the runs were repeatable and that the droplets did not traverse the entire length of the gradient.

5.2. Droplets Stop When the "Difference in Slopes" Reaches a Critical Value. On each gradient surface, we carried out several runs by varying the volume of the droplets but keeping the frequency and amplitude of vibration constant. We noticed that droplets of different volumes came to a halt at different location on the same gradient. To analyze this behavior, we begin by identifying appropriate variables and then create predicted plots using the model and finally plot the observations to make a comparison.

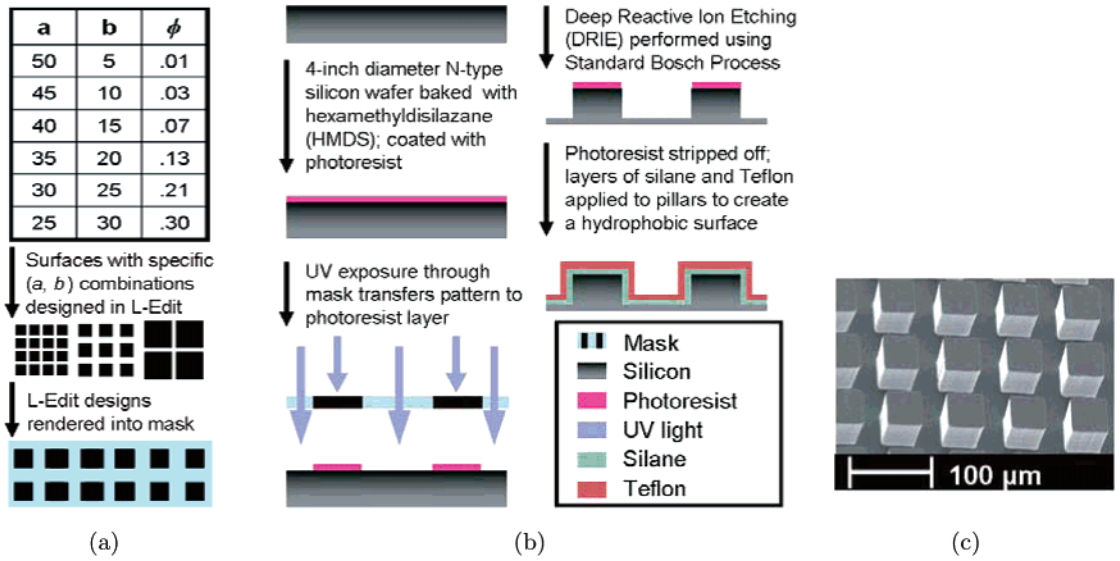

Figure 7. Fabrication process for the test surface. (a) Design of the surface. The (a, b) values for the designed gradients were laid out using L-Edit and printed to create transparency masks. (b) Fabrication of the surface: Photolithography with an AZ4620 resist was followed by DRIE using the standard Bosch process. Etch depths ranged from 70 to 80 μm. The wafer was cleaned, and a hydrophobic coating of Teflon AF 1600 was applied. (c) SEM micrograph of pillars etched in silicon. Each die consisted of two parallel, oppositely oriented, 4-mm-wide gradients 1 mm apart. The gradient tracks were surrounded by a forbidden region with $\phi < \phi_{min}$ to prevent droplets from leaving the gradient track.

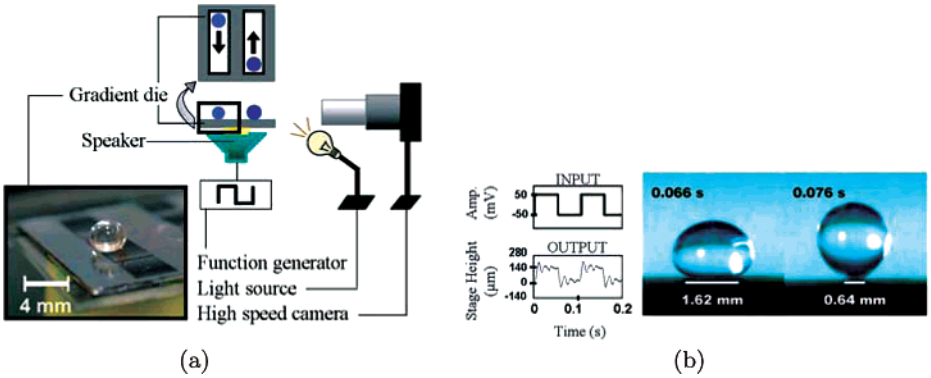

Figure 8. (a) Droplet surface vibrated by a speaker powered by a function generator set at 20 Hz with a 50 mV amplitude. A Gemini high-intensity light source illuminates the droplet. A DRS camera records the movies at 500 fps. (b) Variation of the footprint of a 5 μL droplet for the square wave excitation of the speaker shown in part a.

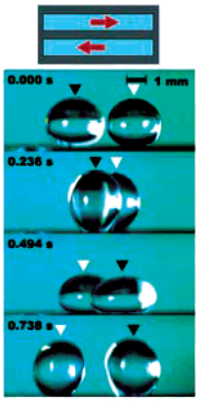

Figure 9. Droplets on oppositely oriented gradients on the same die, when vibrated, traveling in opposite directions down their respective gradients. The droplets were similar in volume (left, 7.67 μL; right, 6.35 μL).

For a given droplet size, the driving force that it experiences is determined by the slope and the random force due to vibration. Hysteresis, which is dependent on the surface structure, determines the impeding force. We employ the model developed in eq 16 to plot the slope required for a 5 μL droplet to begin to move on the continuous gradient shown in Figure 5. The actual slope is also plotted; it is evident that the droplet cannot move without the mitigating help of vibration. For the purpose of this discussion, we call the difference between the slope required for incipient movement and the actual slope at a given location as the "difference of slopes" or simply the "gap". The gap for a droplet at a location on a gradient is a measure of the additional force required to make it move. We use our model to create Figure 11a, which is a plot of gap versus location on the gradient for different droplet volumes. As the gap increases, more force will be required to make the droplet move. Alternately, if we apply a constant force to the droplet, then the droplet will stop when the gap increases to an "upper-limit" value. It can be seen that the curves corresponding to different volumes reach the specific upper limit of 0.68 at different locations. We argue that this "upper-limit" value of 0.68 is a measure of the force applied to the droplets due to vibration. We hypothesize that vibration supplies droplets with sufficient force to overcome a critical gap value of less than 0.68; therefore, the points of intersection in Figure 11a denote the locations on the gradient where the droplets of various volumes come to a halt. Strictly, the force balance is

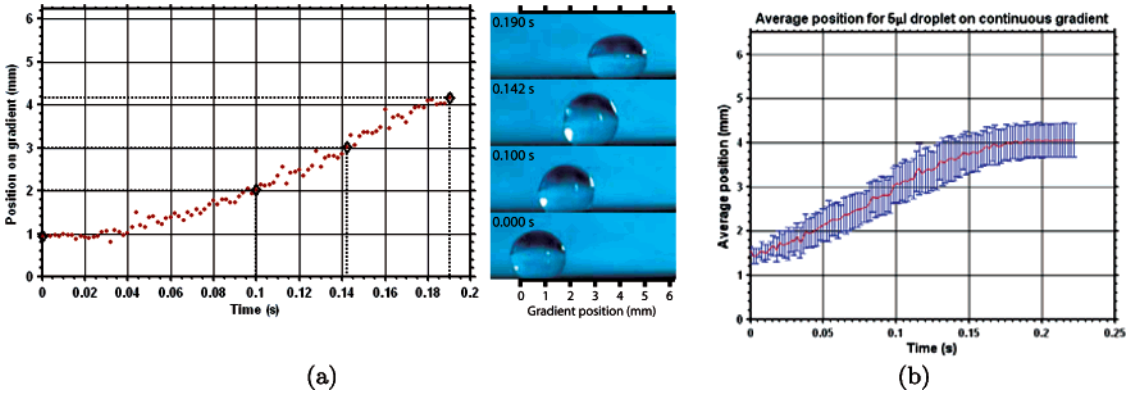

Figure 10. (a) Position of the center of a 4.96 μL droplet plotted as a function of time. Black diamonds mark the movie frames shown at the right as the droplet moves down the 6.24-mm-long gradient. A black ruler above and below the images indicates the length and location of the gradient in the images. (b) Average position of various droplets on the gradient plotted as a function of time. We plot data for the part of the gradient that all droplets have in common (i.e., after the first 1.45 mm of the gradient).

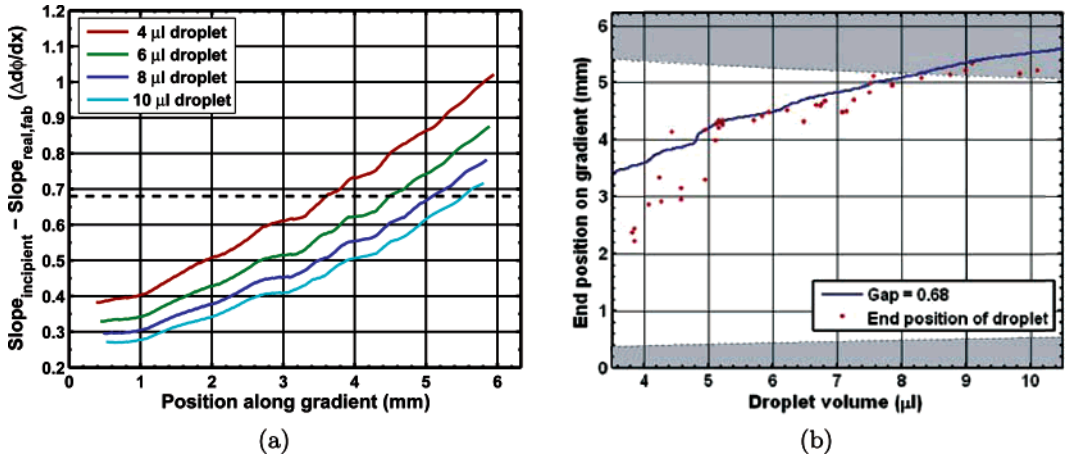

Figure 11. (a) Difference between the slope required for incipient motion and the actual value of the gradient (gap) as a function of $\phi(x)$ for the continuous gradient. A larger gap implies that a larger additional force is required to move the droplet. Smaller droplets had larger gaps at each location; they reached the critical value for the gap ($\Delta d\phi/dx = 0.68$) earlier in the gradient than did larger droplets. (b) Solid line showing the predicted stop location (where the gap first increased to the critical value of 0.68) plotted as a function of droplet volume. Experimentally observed stop locations of the droplets, measured at the center of the droplet, are plotted as red points. The gray regions indicate the effective end of the gradient (i.e., if the center of the droplet were positioned in these regions, then from eq 17 it is evident that part of the droplet base could cross the end of the gradient).

valid at the point where the droplet just begins to decelerate. We make simplifying assumptions that the force balance is valid at the stopping location, neglecting the drag force and the distance over which the droplet decelerates to a halt.

To test our hypothesis, we plot a curve using these predicted "stop" locations of the various sized droplets as a function of their volume, as shown in Figure 11b. We plot the experimentally obtained stop positions for droplets of several volumes. As evident from Figure 11b, the good fit validates the capability of our analytical model to predict trends.

6. Conclusions

This work provides design rules for exploiting physical texture, specifically the solid−liquid contact area fraction ϕ, to create surface-energy gradients that guide droplets along desired trajectories. We have developed an analytical model based on the current theory of wetting of rough surfaces. This model accounts for contact angle hysteresis and predicts the slope required for spontaneous movement of the droplet. We have demonstrated proof-of-principle results along with some trends and showed that the observed trends can be predicted from the model.

While this work introduces hard-coded gradients where droplets are propelled by vibration, it also lays the foundation for completely programmable gradients. Electrically controlled gradients steep enough to overcome hysteresis would move with the droplet to control it. Electrowetting could be the choice of technology to dynamically control the solid−liquid area of Fakir droplets,[33] eventually leading to completely programmable CMOS-compatible microfluidic platforms.

Acknowledgment. This work is funded by NIH Center of Excellence in Genomic Science and Technology grant 1-P50-HG002360-01. A.S. thanks Sidhartha Goyal for useful technical discussions. M.J.C. thanks the UWEB REU program at the University of Washington, which made this association possible. K.F.B. acknowledges a fellowship from the Japan Society for the Promotion of Science (JSPS). He thanks M. Esashi (Tohoku University), H. Fujita (University of Tokyo), and O. Tabata (University of Kyoto) for their generous hospitality during his stay at their laboratories.

LA0601657

(33) Krupenkin, T. N.; Taylor, J. A.; Schneider, T. M.; Yang, S. *Langmuir* **2004**, *20*, 3824−3827.